Short Article

Interferon Regulatory Factors Are Transcriptional Regulators of Adipogenesis

Jun Eguchi,[1,5] Qing-Wu Yan,[1,5] Dustin E. Schones,[2] Michael Kamal,[3] Chung-Hsin Hsu,[1] Michael Q. Zhang,[2] Gregory E. Crawford,[4] and Evan D. Rosen[1,3,*]

[1]Division of Endocrinology and Metabolism, Beth Israel Deaconess Medical Center, Boston, MA 02215, USA
[2]Cold Spring Harbor Laboratory, Cold Spring Harbor, NY 11724, USA
[3]Broad Institute of MIT and Harvard, Cambridge, MA 02142, USA
[4]Institute for Genome Sciences & Policy and Department of Pediatrics, Duke University, Durham, NC 27708, USA
[5]These authors contributed equally to this work.
*Correspondence: erosen@bidmc.harvard.edu
DOI 10.1016/j.cmet.2007.11.002

SUMMARY

We have sought to identify transcriptional pathways in adipogenesis using an integrated experimental and computational approach. Here, we employ high-throughput DNase hypersensitivity analysis to find regions of altered chromatin structure surrounding key adipocyte genes. Regions that display differentiation-dependent changes in hypersensitivity were used to predict binding sites for proteins involved in adipogenesis. A high-scoring example was a binding motif for interferon regulatory factor (IRF) family members. Expression of all nine mammalian IRF mRNAs is regulated during adipogenesis, and several bind to the identified motifs in a differentiation-dependent manner. Furthermore, several IRF proteins repress differentiation. This analysis suggests an important role for IRF proteins in adipocyte biology and demonstrates the utility of this approach in identifying *cis*- and *trans*-acting factors not previously suspected to participate in adipogenesis.

INTRODUCTION

Adipogenesis involves a sequential and ordered cascade of gene expression events coordinated by transcription factors that simultaneously induce tissue-specific gene expression and repress alternate cell fates (Rosen and MacDougald, 2006). In adipogenesis, attention has focused on the nuclear receptor PPARγ and several members of the C/EBP family of bZIP proteins, including C/EBPα, β, and δ. More recently, other proadipogenic factors have been identified, including KLF and EBF proteins (Oishi et al., 2005; Jimenez et al., 2007; Mori et al., 2005). Transcriptional repressors of adipogenesis have also been identified, such as GATA2, GATA3, and KLF2 (Tong et al., 2000; Wu et al., 2005). These pro- and antiadipogenic proteins, working in concert with a number of transcriptional cofactors, integrate a wide array of cellular inputs to determine whether a precursor cell will initiate and complete the differentiation process (Rosen and MacDougald, 2006; Farmer, 2006).

There have been significant recent advances in our ability to define transcriptional pathways in development, brought about by new experimental methods as well as computational approaches (Elnitski et al., 2006). Some of these techniques are amenable to high-throughput analysis, such as the combination of chromatin immunoprecipitation (ChIP) with microarrays (ChIP-chip), but require advance knowledge of which transcription factors may be involved (Negre et al., 2006; Weinmann, 2004). Other methods, like promoter analysis and electrophoretic mobility shift assays (EMSAs), are not easily adaptable to high-throughput format. Several computational techniques have been devised to assist in motif recognition (Ji and Wong, 2006), and although many of these algorithms have been successful at identifying already known *cis* elements, there has been less success in predicting novel pathways. An additional problem with most purely computational approaches is lack of specificity: typically, many more binding sites are predicted than actually participate in bona fide gene expression events.

Mapping DNase hypersensitive sites (DHSs) can be used to identify *cis* elements with important biological functions (Krebs and Peterson, 2000). This method relies on the ability of small amounts of DNase I to digest regions of open or accessible chromatin. These regions are often associated with protein binding and include enhancers, promoters, silencers, insulators, and locus control regions. Despite the ability of DNase hypersensitivity analysis to identify important *cis*-acting elements, only a few hundred such sites have been identified over a quarter of a century. Limitations of the technique include the need for iterative Southern blotting, relatively large amounts of starting material, and significant radiation use. A few groups have improved upon the traditional approach to DNase hypersensitivity by adapting it to high-throughput technologies like quantitative polymerase chain reaction (qPCR), massively parallel signature sequencing, and tiled microarrays (McArthur et al., 2001; Crawford et al., 2004, 2006a, 2006b; Sabo et al., 2004, 2006; Bernat et al., 2006).

Here, we used a qPCR-based DNase hypersensitivity strategy to look for regulatory elements involved in adipocyte differentiation. This approach yielded sites that were used as input sequences in a computational algorithm designed to identify overrepresented motifs involved in tissue-specific gene expression. One top-scoring motif corresponded to a binding site for interferon regulatory factors (IRFs). We show that IRFs are expressed in fat, are developmentally regulated, and bind to
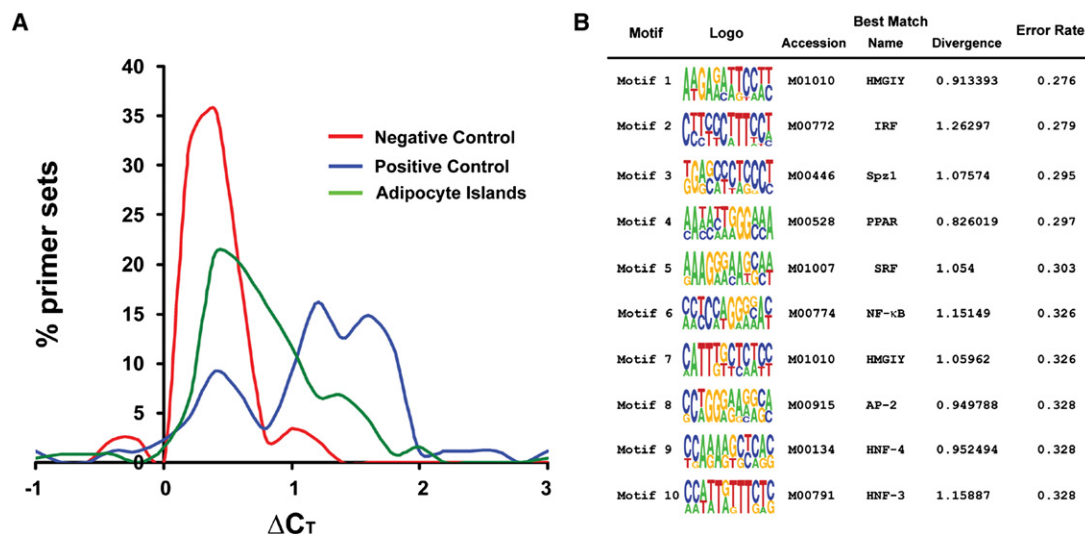
Figure 1. DNase Hypersensitive Sites Can Be Identified Flanking Adipocyte-Selective Genes

(A) DNase hypersensitivity results for day 7 adipocytes. The x axis represents the difference in cycle threshold (ΔC_T) between DNase-digested and undigested samples. The y axis represents the percent of all primer sets that displayed any given ΔC_T. The red line corresponds to random primers (negative control). The blue line corresponds to primers that amplify known DNase hypersensitive sites (DHSs) in other cell types (positive control). The green line describes results using primer pairs derived from the adipocyte-selective gene set. See text for details.

(B) Top motifs identified by the computational algorithm DME in differentiation-dependent DHSs, ranked by error rate. The information displayed includes the sequence logo; the best matching TRANSFAC profile including the accession number, the name of the TRANSFAC profile, and the Kullback-Leibler (KL) divergence score of the discovered motif and the TRANSFAC motif; and the error rate.

the predicted *cis* elements. Furthermore, some IRFs repress the entire adipogenic process. Taken together, these studies demonstrate the utility of integrating experimental and computational techniques to identify factors and pathways in cellular differentiation and tissue-specific gene expression.

RESULTS

qPCR-Based DNase Hypersensitivity Analysis of Adipocyte Genes

We chose to study 27 genes that possessed two key characteristics: (1) expression limited to very few tissues, including brown and/or white adipose tissue, and (2) expression induced during adipogenesis (see Figure S1 available online). DHSs are enriched in the proximal 50 kb upstream of the transcriptional start site (TSS) and in the first intron (Crawford et al., 2006b), so we restricted our search to these areas. Areas of high conservation and at least 70 bp in length were chosen on the assumption that important regulatory sites tend to be clustered together, giving them a size larger than the typical 6- to 10-mer bound by an individual transcription factor (Elnitski et al., 2006). Overall, we identified 268 such regions flanking our genes of interest (Table S1); these regions were used to design PCR primers.

We next harvested nuclei from 3T3-L1 cells prior to differentiation (day 0) and after conversion to mature adipocytes (day 7) (Figure S2). Nuclei were exposed to variable concentrations of DNase I, and samples were selected for further analysis based on similarity of degree of digestion (Figure S2). In addition to the 268 primer sets mapping to adipose-selective genes, we also tested primer sets randomly distributed throughout the mouse genome (negative control) and primer sets flanking DHSs found in several other cell types (positive control).

The critical parameter for each region is the difference in amplification cycle threshold (ΔC_T) between samples treated with and without DNase I. A high ΔC_T means that DNase I mediated template reduction and implies the existence of a DHS within the amplicon; a low ΔC_T suggests the opposite. Data from day 7 samples are shown in Figure 1A. As expected, randomly selected regions are generally not hypersensitive and display a low ΔC_T, while sites that are hypersensitive in nonadipose tissues also show a rightward shift in adipocytes. The adipocyte-selective set displays an intermediate pattern. Comparing the ΔC_T at day 0 (Figure S3) to the ΔC_T at day 7 allowed us to determine which DHSs show differentiation dependence. There were 32 such regions, mapping to 14 of the original 27 genes (51.9%; see Table S2).

Initial Characterization of Differentiation-Dependent DHSs

One of the DHSs was *Fabp4 I8* (identified by gene and "island" or "I" number). This region contains two well-validated PPARγ binding sites and is the key element required for adipose-specific expression of FABP4 (Graves et al., 1992; Tontonoz et al., 1994). The presence of this region among our differentiation-dependent DHSs served as an unintended positive control. We estimated the size of this DHS at approximately 1 kb by designing primers flanking both sides of the site at 700 bp intervals (Figure S4), in accordance with the size of DHSs reported elsewhere (Frenster, 1976).

Our next goal was to confirm that differentiation-dependent DHSs display properties associated with transcriptional regulation. We first looked at histone modification in some of these regions using ChIP. Fifteen of 21 DHSs tested showed a differentiation-dependent accumulation of acetyl groups on histone 3 (H3), a modification associated with transcription factor binding sites (Figure S5) (Villar-Garea and Imhof, 2006). We also tested
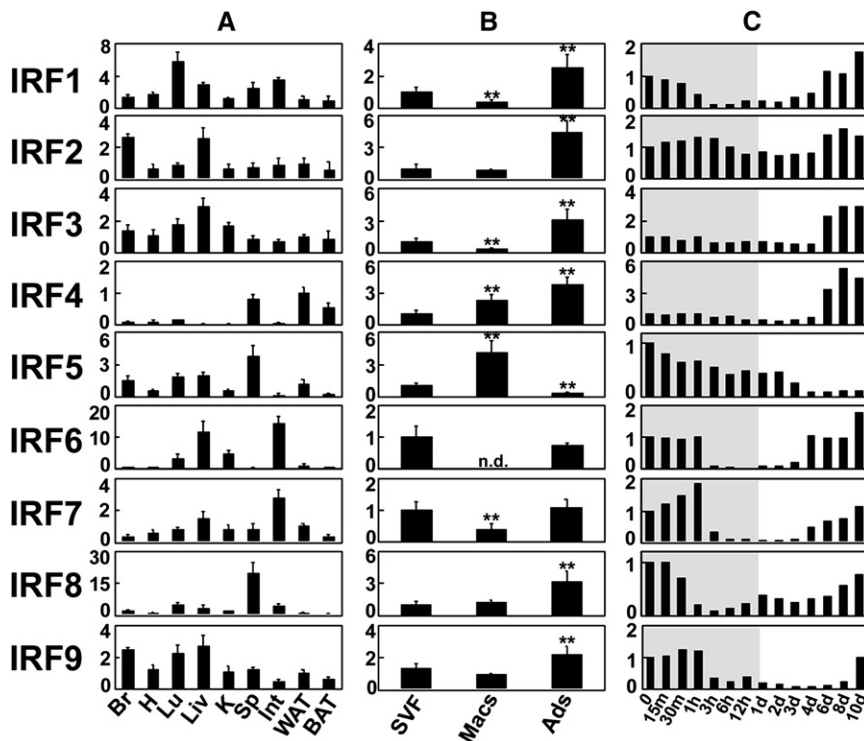
Figure 2. IRFs Are Expressed in Adipose Tissue In Vivo and In Vitro

(A) qPCR-based expression of IRF1–9 in tissues from male FVB mice. Br, brain; H, heart; Lu, lung; Liv, liver; K, kidney; Sp, spleen; Int, intestine; WAT, white adipose tissue; BAT, brown adipose tissue. Data are expressed as mean ± SEM fold induction relative to IRF mRNA expression in WAT; all values are normalized to *36B4* expression. n = 3.

(B) IRF expression was assessed in samples of fractionated fat pads from C57BL/6 mice. SVF, stromal-vascular fraction; Macs, F4/80+ macrophages; Ads, adipocytes. Data are expressed as mean ± SD fold induction relative to IRF mRNA expression in SVF. n = 6, **p < 0.01 versus SVF; n.d., not detectable.

(C) IRF expression during 3T3-L1 differentiation. Note that the time scale is not linear; the shaded area indicates time points <24 hr. Data are normalized to *36B4* expression and are expressed as fold induction relative to IRF mRNA at day 0.

the ability of DHSs to bind factors from adipocyte nuclear extracts. All four sites tested bound to factors from 3T3-L1 adipocytes, and three of the four formed complexes more efficiently with day 7 extracts than with extracts from day 0 preadipocytes (Figure S7 and data not shown).

Computational Analysis of Hypersensitive Sites Identifies Relevant *cis* Motifs

In order to identify factors that bind to DHSs, we used a computational algorithm called Discriminating Matrix Enumerator (DME) that has shown promise in identifying tissue-specific transcriptional pathways (Smith et al., 2005). DME chooses motifs that best distinguish between two sequence sets; in this case, we compared DHSs to randomly selected sequences from the regions surrounding the DHSs. The top ten DME-discovered motifs and their best matching TRANSFAC profiles are shown in Figure 1B. Interestingly, two of the top-scoring hits were motifs for HMGI-Y, a protein already known to participate in adipogenesis (Melillo et al., 2001). Similarly, a PPAR motif also scored highly, as did a NF-κB motif. These factors are well known to activate and inhibit adipocyte gene expression, respectively (Tontonoz et al., 1994; Ruan et al., 2003). Among the top-scoring motifs was a binding site for IRFs. The Search Tool for Occurrences of Regulatory Motifs (STORM) (Schones et al., 2007) was used to predict putative IRF response elements (IRF-REs) corresponding to this IRF profile (Table S3).

IRFs Are Expressed in Adipose Tissue and Regulated during Differentiation

Mammals possess nine distinct IRF genes, which play key roles in several aspects of the immune response (Taniguchi et al., 2001; Lohoff and Mak, 2005). There have been no reports, how-

ever, of IRF expression or function in adipocytes. Using qPCR, we ascertained that all IRF isoforms are expressed in murine adipose tissue (Figure 2A). IRF4 was particularly interesting in that it showed relative tissue specificity for adipose tissue and spleen. These data were confirmed using northern blotting for all IRFs (Figure S6A) and western blotting for IRF4 (Figure S6B).

Adipose depots contain immune cells, raising the issue of whether IRFs are expressed in adipocytes per se. White adipose pads were fractionated into adipocytes, macrophages, and stromal-vascular cells, and expression of IRF isoforms was measured using qPCR (Figure 2B). All IRFs were expressed in the adipocyte fraction, and all except IRF5 were more highly expressed in adipocytes than in resident macrophages.

Interestingly, all nine IRFs show developmental regulation during adipogenesis in cultured fat cells (Figure 2C), generally falling into three distinct expression patterns. Most IRFs (IRF1, IRF2, IRF6, IRF7, IRF8, and IRF9) are expressed in preadipocytes and are then repressed early after the induction of differentiation before becoming re-expressed in mature adipocytes. The expression of IRF3 and IRF4 is induced during differentiation. Finally, IRF5 is highly expressed in preadipocytes but disappears as adipogenesis proceeds.

IRFs Bind to Predicted Motif Regions in DHSs In Vitro and In Vivo

To determine whether IRF proteins bind to identified motifs within DHSs, we used ChIP analysis in cells at day 0 or day 7 after the induction of differentiation, focusing on IRF1, IRF2, IRF3, IRF4, and IRF8 due to the availability of suitable antibodies. Figure 3A shows that several IRFs bind to the predicted DHSs, many in a developmentally regulated manner. For example, *Acdc I5* and *Aoc3 I1* show significantly more IRF binding in
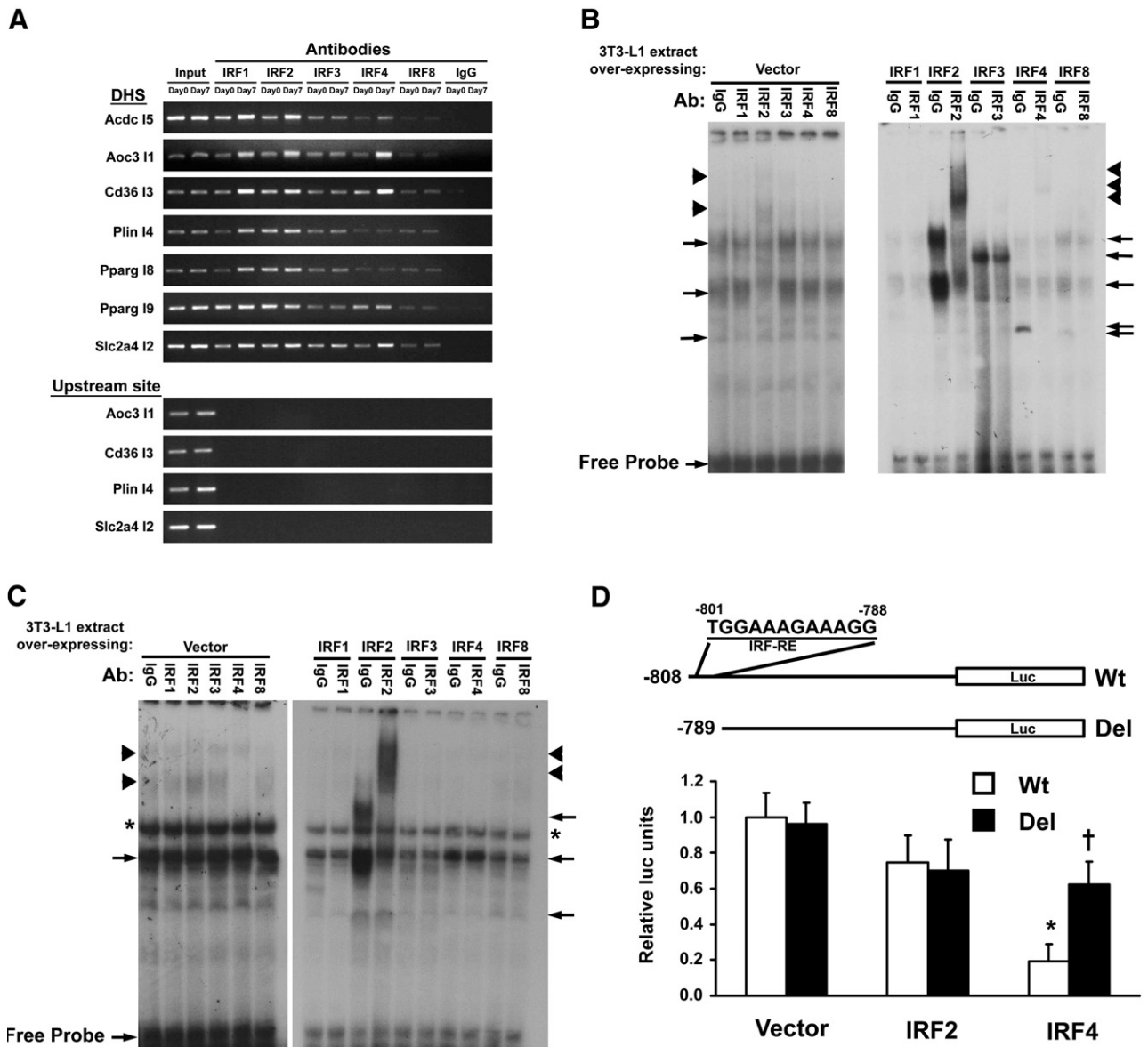
Figure 3. IRFs Bind to Regions Identified by DME

(A) Binding of IRFs to DHSs in adipocytes using ChIP. Data are representative of three experiments.

(B) EMSA using *Cd36 I3* as the probe. Left: extract from day 0 3T3-L1 preadipocytes was coincubated with radiolabeled *Cd36 I3* probe and an IRF-specific antibody or IgG. Right: a similar experiment using cells transfected with IRF-expressing plasmids. In (B) and (C), arrows denote complexes containing IRF isoforms, while arrowheads denote an antibody-mediated supershift. Asterisks in (C) indicate a complex of uncertain provenance.

(C) EMSA using *Slc2a4 I2* as the probe. Left: extract from day 0 cells was coincubated with labeled *Slc2a4 I2* probe and an IRF-specific antibody or IgG. Right: a similar experiment using cells transfected with IRF-expressing plasmids.

(D) The murine *Slc2a4* promoter is shown with the IRF response element (IRF-RE) from −801 to −788 (top). Constructs with and without the IRF-RE were cotransfected into day 5 3T3-L1 adipocytes with plasmids expressing IRF2, IRF4, or empty vector, and luciferase expression was determined 24 hr later. Results are expressed as mean ± SD (n = 3). *p < 0.05 relative to vector control; †p < 0.05 relative to wild-type (Wt) promoter.

day 7 adipocytes than in day 0 preadipocytes. Other DHSs, such as *Plin I4* and *Pparg I9*, show constitutive IRF binding in both developmental states.

EMSAs were employed to further characterize the binding of specific IRFs to the predicted motifs. For the *Cd36 I3* motif, for example, enhanced complex formation was seen using nuclear extracts prepared from 3T3-L1 cells overexpressing IRF2, IRF3, IRF4, and IRF8 (Figure 3B), all of which were also shown

to bind this region in the ChIP assay. Using antibodies against these factors, we were able to demonstrate supershifting of complexes containing IRF2, IRF4, and IRF8 and diminution of the complex containing IRF3. Supershifting of IRF2 is also visible in the absence of ectopic overexpression. Similarly, when the probe was switched to the putative IRF-RE from the *Glut4* gene (*Slc2a4 I2*), we observed enhanced complex formation with IRF2 and IRF4 and supershifting with anti-IRF2 (Figure 3C).

Other putative IRF motifs were also shown to bind to multiple IRFs, including *Pparg I8*, *Pparg I9*, and *PlinI4* (data not shown). For *Pparg I8*, we used a consensus IRF-RE to successfully compete for binding to a factor in day 7 extract; a mutant consensus motif was ineffective (Figure S7).

Finally, we generated a construct in which luciferase is driven by the −808 bp murine *Slc2a4* promoter, containing the putative IRF motif at the distal end. Cotransfected IRF4, but not IRF2, repressed expression from this construct (Figure 3D). A small deletion eliminating only the putative IRF motif prevented IRF4 from repressing luciferase expression. Taken together, the ChIP, EMSA, and transactivation assay data indicate that these putative motifs are bona fide IRF binding sites.

IRFs Are Endogenous Regulators of Adipogenesis and Adipocyte Gene Expression

We next sought to determine whether IRFs play a functional role in adipocyte differentiation. IRF isoforms were introduced by retroviral transduction into 3T3-L1 preadipocytes, which were then treated with dexamethasone, methylisobutylxanthine, and insulin (DMI) (see Figure S8A and Table S6). IRF3 and IRF4 were the only isoforms with a significant effect on lipid accumulation (Figure 4A) and terminal gene expression (Figure 4B). All other IRF isoforms repressed at least one nonoverlapping target gene, suggesting specificity in the IRF transcriptional response.

We also performed studies using lentiviral delivery of short hairpin RNAs (shRNAs) directed against individual IRF isoforms in 3T3-L1 preadipocytes (Figure S8B). We were unable to identify a specific hairpin that reduced levels of IRF4 or IRF8 despite extensive efforts; these two factors are thus excluded from this analysis. Of the remaining IRFs, only IRF1 and IRF3 knockdown provoked consistently elevated oil red O staining (Figure 4C). Reduction of IRF1 and IRF3 during differentiation also resulted in enhanced adipocyte gene expression (day 7 results are shown in Figure 4D; see Figure S9 for full time-course data), including PPARγ and C/EBPα. Consistent with the overexpression experiments, all other IRFs tested except IRF5 showed an effect on one or more individual genes.

We also asked whether IRFs might affect adipocyte gene expression outside of the context of differentiation. Transient transfection of IRF expression constructs was performed in 3T3-L1 adipocytes 5 days after DMI treatment, with gene expression assessed on day 7. We examined the expression of eight adipocyte target genes, including those for which an IRF-RE was predicted by the DNase hypersensitivity analysis. All IRF isoforms repressed adipocyte-specific gene expression (Figure S11A). However, most IRF family members are activators of gene expression in immune cells. We thus measured levels of known immune-related IRF target genes (e.g., *Ifna*, *Ccl5*, *Cxcl9*, *Gata3*, and *Il15*) in the setting of IRF overexpression in adipocytes. These genes were generally activated by IRF overexpression, and in no case was repression seen (Figure S11B). These results indicate that IRFs do not generally reduce gene expression in adipocytes but rather repress adipocyte-specific gene expression selectively.

Finally, we performed analogous loss-of-function experiments by transfecting mature (i.e., day 5) adipocytes with shRNA directed against specific IRF isoforms (Figure S10). In the case of IRF4, the absence of an identifiable shRNA construct led us

to employ a siRNA SMARTpool (Dharmacon) instead. As predicted, expression of most of the adipocyte-specific genes was enhanced by IRF knockdown (Figure S11C). Some target genes showed specificity for a limited number of IRFs; for example, *Plin* and *Pparg* were enhanced only by reduction of IRF3, and *Cd36* and *Slc2a4* were affected only by IRF3 and IRF4. Other genes, such as *Acdc* and *Fabp4*, were affected by larger (but not completely overlapping) sets of IRFs, again suggesting specificity of IRF action in adipocytes.

DISCUSSION

This study reports the integrated use of DNase hypersensitivity analysis, computational algorithms, and experimental biology to predict and confirm transcriptional regulators. A particular strength of this study is the use of cells pre- and postdifferentiation, which allowed temporal changes in DHSs to be used to select for regulators with an impact on the developmental process.

The qPCR-based method of DNase hypersensitivity analysis requires a priori selection of regions of interest, which necessarily introduces some bias. An alternative strategy is to use overlapping sets of primers, which can achieve complete coverage of a given region. This approach lacks practicality, however, when applied to large stretches of sequence such as we used here. It is expected that array-based detection or Solexa sequencing of DHSs will ultimately solve this problem (Crawford et al., 2006a; Sabo et al., 2006). For the current study, we introduced certain biases to make the project tractable. First, the choice of genes was justified on the basis of their adipose selectivity and their induction during adipogenesis. There are many more genes expressed in adipocytes, and their inclusion would increase the robustness of the analysis. Second, we limited the regions of study to the proximal upstream 50 kb and the first intron. These regions are enriched for DHSs, but relevant sites can certainly exist in other locations as well, such as 3′ flanking sequence, other introns, and distal intergenic regions. Finally, we imposed a somewhat arbitrary size and conservation cutoff (70 bp and 70% identity across species). Approximately 60% of DHSs are located in such highly conserved regions, but many sites of interest are either species specific or display less conservation than required here (Crawford et al., 2006b).

Despite these limitations, we were able to rapidly increase the number of known adipose differentiation-dependent DHSs. These sites accumulate acetylated histones over the course of adipose conversion and bind to adipocyte nuclear proteins. The size of one DHS was measured and found to be approximately 1 kb in length, consistent with the reported size of many other such regions (Frenster, 1976). These characteristics suggest that the DHSs we identified are bona fide transcription factor binding sites.

Our goal was not simply to characterize new adipose-specific DHSs, however, but to identify transcriptional pathways that regulate adipocyte gene expression. We therefore employed a computational algorithm (DME) to identify overrepresented motifs in the DHSs, several of which correlated with transcription factors associated with adipogenesis, including HMGI-Y, PPARγ, and NF-κB. The presence of a putative IRF binding site among the top-scoring motifs, however, was a surprise, as these well-studied proteins have not been described in fat.
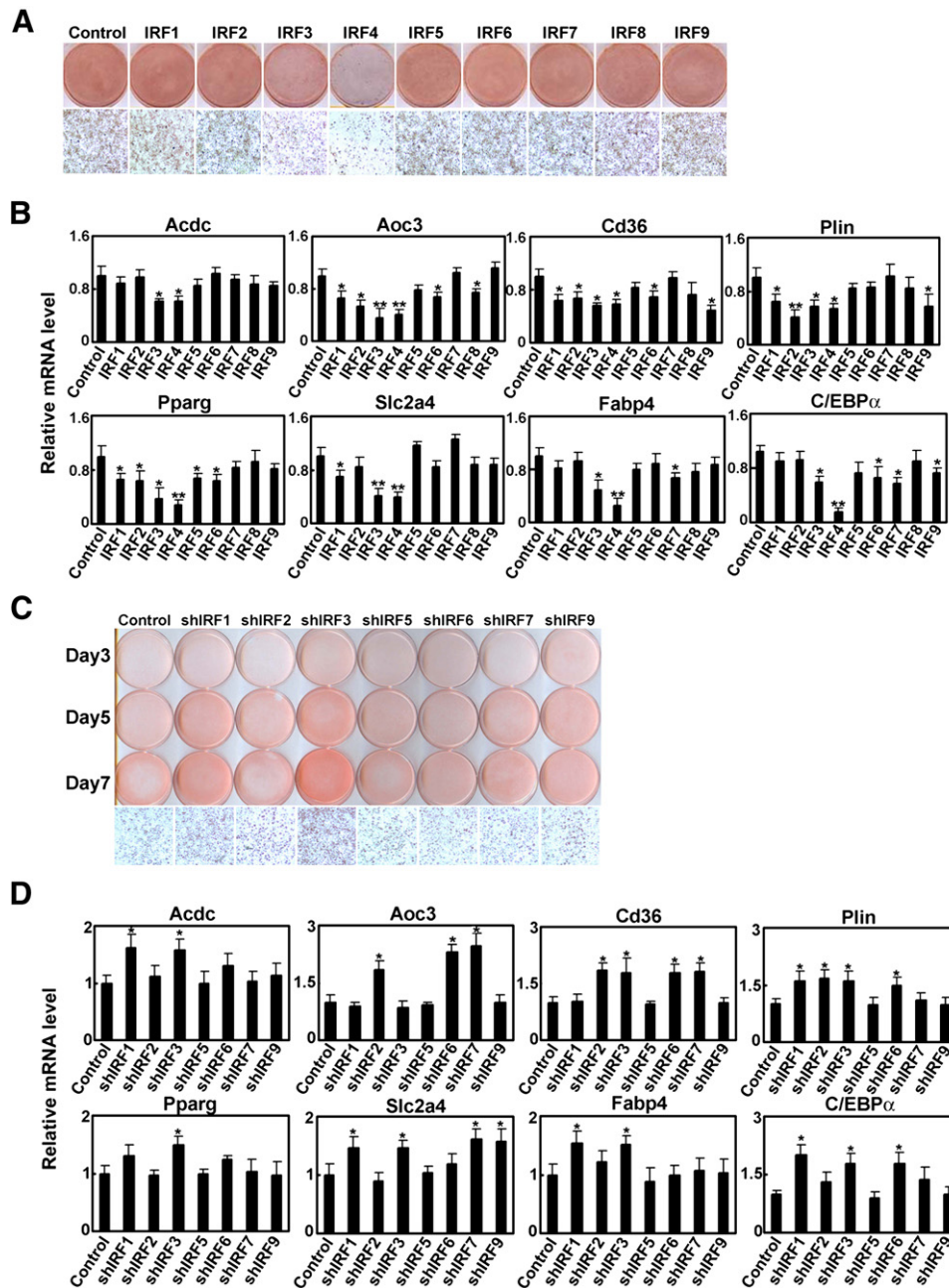
Figure 4. IRF Proteins Repress Adipogenesis

(A) 3T3-L1 preadipocytes were transduced with retroviruses expressing IRFs and differentiated with dexamethasone, methylisobutylxanthine, and insulin (DMI). Cells were stained with oil red O 7 days post-DMI treatment.

(B) Cells shown in (A) were harvested at day 7 post-DMI treatment, and qPCR was used to determine levels of adipocyte genes relative to control cells. All samples are normalized to *36B4*. Results are expressed as mean ± SD (n = 3). *p < 0.05, **p < 0.01 versus vector control.

(C) 3T3-L1 preadipocytes were transduced with lentiviruses expressing shRNAs directed against the indicated IRF isoforms. Oil red O staining was performed at days 3, 5, and 7 post-DMI treatment.

(D) Cells shown in (C) were harvested at day 7 post-DMI treatment, and qPCR was used to determine levels of adipocyte genes relative to control cells. All samples are normalized to *36B4*. Results are expressed as mean ± SD (n = 3). *p < 0.05, **p < 0.01 versus vector control.

All nine mammalian IRFs are expressed in murine adipocytes, and all show developmental regulation during adipogenesis. Some IRFs (e.g., IRF4) even display relative specificity for adipose tissue. Importantly, we show that IRFs not only are expressed in adipocytes but bind to the sequences predicted by DME and repress adipogenesis. This is particularly true of IRF3 and IRF4, though all IRFs other than IRF5 appear to have some effect when specific adipocyte genes are examined. This suggests that different IRF isoforms have distinct yet overlapping roles in adipogenesis and in regulating gene expression in

mature cells. The repressive action of IRF in adipocytes is entirely consistent with their inclusion in DHSs, which often contain silencer elements (Dirks et al., 1993; Tanaka et al., 1998; Hermann and Heckert, 2005). It is worth noting that the actions of IRF3, IRF4, and some other members of this family are similar to those of NF-κB, another transcription factor that activates immunoregulatory genes and represses adipocyte-specific gene expression.

IRFs have mainly been studied in the context of immune regulation, and there is growing appreciation of the importance of inflammatory pathways in adipocytes, which are generally associated with insulin resistance (Hotamisligil, 2006). For example, inflammatory signals and fatty acids are both ligands for toll-like receptor 4 (TLR4), which mediates reduced insulin action in fat cells (Shi et al., 2006). In macrophages and other immune cells, TLRs exert many of their effects through changes in IRF activity, and we speculate that IRFs may mediate the effects of TLR4 (or other TLRs) in adipocytes (Taniguchi et al., 2001; Lohoff and Mak, 2005). Interestingly, IRF3 has been shown to repress retinoid X receptor (RXR)- and liver X receptor (LXR)-mediated signaling in hepatocytes and macrophages, respectively (Castrillo et al., 2003; Chow et al., 2006). A similar effect in adipocytes would be predicted to reduce gene expression associated with lipid storage and other key adipose functions, consistent with our findings of repression of adipocyte genes. IRFs mediate their actions in immune cells through a complex series of protein-protein interactions and posttranslational modifications (Taniguchi et al., 2001; Lohoff and Mak, 2005). We are currently investigating these issues in adipocytes, in addition to determining the metabolic consequences of IRF action in vivo.

In summary, these studies demonstrate the power of an integrated computational and experimental approach to identify transcriptional regulators. DNase hypersensitivity analysis in particular can be a useful method to study the simultaneous regulation of multiple genes involved in development and physiology.

EXPERIMENTAL PROCEDURES

Cell Culture
3T3-L1 cells were cultured in DMEM with 10% BCS in 5% CO_2. Two days postconfluence, cells were exposed to DMEM/10% FBS with dexamethasone (1 μM), insulin (5 μg/ml), and isobutylmethylxanthine (0.5 mM). After 2 days, cells were maintained in medium containing insulin and FBS until ready for harvest at day 7.

Generation of Retroviral Constructs
The coding regions of mouse IRFs were isolated from 3T3-L1 adipocyte mRNA by RT-PCR using TaKaRa Ex Taq polymerase (Takara Bio Inc.) and subcloned into pMSCV (Clontech). To generate IRF-pMSCV expression vectors, *IRF1*, *IRF4*, *IRF8*, and *IRF9* cDNAs were cloned into the BglII and EcoRI sites of the pMSCV vector. *IRF3*, *IRF6*, and *IRF7* cDNAs were cloned into the XhoI and EcoRI sites of the pMSCV vector. *IRF2* cDNA was cloned into the XhoI and HpaI sites of the pMSCV vector. *IRF5* cDNA was cloned into the HpaI and EcoRI sites of the pMSCV vector.

Transfection
Five days after adipogenic stimulation, 3T3-L1 cells were detached with trypsin and transfected with 4 μg of IRF-pMSCV or empty pMSCV along with 0.1 μg of EGFP expression vector using the Amaxa nucleofection system (Amaxa Biosystems). Cells were then cultivated in DMEM/10% FBS. Forty-eight hours posttransfection, RNA was harvested and subjected to qPCR. For experiments with shRNA, day 5 3T3-L1 adipocytes were transfected with shRNA constructs as described below. For IRF4, 200 pmol of siRNA oligonucleotide duplexes (Dharmacon) or nontargeting control siRNA was transfected. RNA was harvested 48 hr later and subjected to qPCR.

Animals
FVB mice were obtained from Charles River Laboratories and fed a standard diet (8664, Harlan Teklad). Mice were maintained under a 14 hr light/10 hr dark cycle at constant temperature (22°C) with free access to food and water. For analysis of IRF mRNA expression in various tissues, 10-week-old male FVB mice were used. All animal studies were approved by the Institutional Animal Care and Use Committee of Beth Israel Deaconess Medical Center.

Chromatin Immunoprecipitation
3T3-L1 cells were treated with 1% formaldehyde for 10–15 min at room temperature to crosslink DNA-protein complexes. Genomic DNA was sheared using a Sonic Dismembrator Model 100 (Fisher Scientific) to obtain fragments ranging from 200 bp to 1 kb. ChIP was performed using a kit from Upstate, with 3 μg of primary antibody or rabbit IgG. The following primary antibodies were used: rabbit anti-IRF1 (sc-640), rabbit anti-IRF2 (sc-498), rabbit anti-IRF3 (sc-9082), rabbit anti-IRF4 (sc-6059), and rabbit anti-ICSBP (sc-6058) (Santa Cruz Biotechnology); rabbit anti-Histone H3 (ab1791-100) (Abcam); and rabbit anti-acetyl-histone H3 (06-599) (Upstate). Crosslinking was reversed and purified DNA was subjected to PCR amplification using TaKaRa Ex Taq polymerase. The PCR products were analyzed by electrophoresis on a 3% agarose gel. The primers used for the ChIP assay were the same as those used to amplify the conserved islands (Table S4).

Electrophoretic Mobility Shift Assay
Nuclear extracts were prepared from 3T3-L1 cells during differentiation as described previously (Graves et al., 1992). Oligonucleotide probes (Sigma-Genosys) were labeled with [γ-^{32}P]ATP by T4 polynucleotide kinase (Invitrogen). Binding reactions containing 10 μg of the nuclear extract, ^{32}P-labeled probe (20,000 cpm), and 1 μg of poly(dI:dC) (Sigma) in binding buffer (20 mM HEPES [pH 7.6], 1 mM EDTA, 1 mM dithiothreitol, and 100 mM KCl) were performed at 25°C for 30 min. Samples were run on 4% nondenaturing acrylamide gels in 1× Tris-glycine-EDTA buffer (pH 7.9). Sequences of EMSA probes used were as follows: IRF-RE, 5′-CTCACGCTTTGG**AAA**GTG**AAA**CCTACCTCACTC-3′; IRF-RE (mut), 5′-CTCACGCTTTGG**ACA**GTG**ACA**CCTACCTCACTC-3′; *Ppargl8* putative IRF-RE, 5′-CTTCCCACTTCTCATTTC AATGTGTA-3′; *Cd36 I3* probe, 5′-AGGAAAGGAAAGGAAAGGAAAGGAAA G-3′; *Slc2a4 l2* probe, 5′-TGATCGTCCTTTCTTTCCACGCATCT-3′. For super-shifting studies, extracts were incubated with 10 μg of specific IRF antibody or rabbit IgG (using the same antibodies described above for ChIP assays) on ice for 1 hr before adding labeled probes.

Analysis of Gene Expression by qPCR
Total RNA was extracted from cells using TRIzol reagent (Invitrogen) following the manufacturer's instructions. Fat pads were fractionated into adipocytes, macrophages, and stromal-vascular cells as described in Jimenez et al. (2007). First-strand cDNA synthesis was performed using RETROscript (Ambion). Total RNA was converted into first-strand cDNA using oligo(dT) primers as described by the manufacturer. PCR was performed using cDNA synthesized from 1.5 μg total RNA in an Mx3000P qPCR system (Stratagene) with specific primers and SYBR Green PCR Master Mix (Stratagene). The relative abundance of mRNAs was standardized using *36B4* mRNA as the invariant control. Primers used are listed in Table S3.

Luciferase Reporter Assay
The indicated regions of the murine *Slc2a4* (*Glut4*) promoter were PCR amplified and ligated into pGL3-Basic (Promega). Day 5 3T3-L1 adipocytes were transfected using electroporation as described above. Transfections were performed using 2 μg of reporter construct along with 2 μg of IRF-pMSCV expression vector (or pMSCV alone), along with 0.2 μg of galactosidase expression vector. Luciferase activity was measured 24 hr after transfection using the Galacto-Star luciferase reporter assay (Roche) according to the manufacturer's instructions.

Retroviral Transduction

IRF-pMSCV constructs were transfected into Phoenix packaging cells using the CellPhect transfection kit (Amersham Biosciences). 3T3-L1 preadipocytes were transduced with viral supernatants and then selected in puromycin.

Lentiviral Constructs and Lentiviral Infection

IRF shRNA constructs in pLKO.1 designed by The RNAi Consortium at the Broad Institute were obtained from Sigma. Each shIRF construct was transfected into 293T packaging cells using the CellPhect transfection kit along with a pCMV-dR8.91- and a VSV-G-expressing plasmid. 3T3-L1 cells were transduced with viral supernatants, and cells were selected in puromycin. The constructs chosen for the knockdown experiments were: IRF1, TRC N0000077441; IRF2, TRCN0000071473; IRF3, TRCN0000085242; IRF5, TRCN0000081565; IRF6, TRCN0000085330; IRF7, TRCN0000077290; IRF9, TRCN0000081654.

Statistical Analysis

Unpaired two-tailed Student's t test or one-way ANOVA was used for comparison. $p < 0.05$ was considered statistically significant.

Additional methods can be found in the Supplemental Experimental Procedures.

Supplemental Data

Supplemental Data include Supplemental Experimental Procedures, Supplemental References, eleven figures, and six tables and can be found with this article online at http://www.cellmetabolism.org/cgi/content/full/7/1/86/DC1/.

REFERENCES

Bernat, J.A., Crawford, G.E., Ogurtsov, A.Y., Collins, F.S., Ginsburg, D., and Kondrashov, A.S. (2006). Distant conserved sequences flanking endothelial-specific promoters contain tissue-specific DNase-hypersensitive sites and over-represented motifs. Hum. Mol. Genet. 15, 2098–2105.

Castrillo, A., Joseph, S.B., Vaidya, S.A., Haberland, M., Fogelman, A.M., Cheng, G., and Tontonoz, P. (2003). Crosstalk between LXR and toll-like receptor signaling mediates bacterial and viral antagonism of cholesterol metabolism. Mol. Cell 12, 805–816.

Chow, E.K., Castrillo, A., Shahangian, A., Pei, L., O'Connell, R.M., Modlin, R.L., Tontonoz, P., and Cheng, G. (2006). A role for IRF3-dependent RXRalpha repression in hepatotoxicity associated with viral infections. J. Exp. Med. 203, 2589–2602.

Crawford, G.E., Holt, I.E., Mullikin, J.C., Tai, D., Blakesley, R., Bouffard, G., Young, A., Masiello, C., Green, E.D., Wolfsberg, T.G., et al. (2004). Identifying gene regulatory elements by genome-wide recovery of DNase hypersensitive sites. Proc. Natl. Acad. Sci. USA 101, 992–997.

Crawford, G.E., Davis, S., Scacheri, P.C., Renaud, G., Halawi, M.J., Erdos, M.R., Green, R., Meltzer, P.S., Wolfsberg, T.G., and Collins, F.S. (2006a). DNase-chip: a high-resolution method to identify DNase I hypersensitive sites using tiled microarrays. Nat. Methods 3, 503–509.

Crawford, G.E., Holt, I.E., Whittle, J., Webb, B.D., Tai, D., Davis, S., Margulies, E.H., Chen, Y., Bernat, J.A., Ginsburg, D., et al. (2006b). Genome-wide mapping of DNase hypersensitive sites using massively parallel signature sequencing (MPSS). Genome Res. 16, 123–131.

Dirks, R.P., Jansen, H.J., Onnekink, C., De Jonge, R.J., and Bloemers, H.P. (1993). DNase-I-hypersensitive sites located far upstream of the human c-sis/PDGF-B gene comap with transcriptional enhancers and a silencer and are preceded by (part of) a new transcription unit. Eur. J. Biochem. 216, 487–495.

Elnitski, L., Jin, V.X., Farnham, P.J., and Jones, S.J. (2006). Locating mammalian transcription factor binding sites: a survey of computational and experimental techniques. Genome Res. 16, 1455–1464.

Farmer, S.R. (2006). Transcriptional control of adipocyte formation. Cell Metab. 4, 263–273.

Frenster, J.H. (1976). Selective control of DNA helix openings during gene regulation. Cancer Res. 36, 3394–3398.

Graves, R.A., Tontonoz, P., Platt, K.A., Ross, S.R., and Spiegelman, B.M. (1992). Identification of a fat cell enhancer: analysis of requirements for adipose tissue-specific gene expression. J. Cell. Biochem. 49, 219–224.

Hermann, B.P., and Heckert, L.L. (2005). Silencing of Fshr occurs through a conserved, hypersensitive site in the first intron. Mol. Endocrinol. 19, 2112–2131.

Hotamisligil, G.S. (2006). Inflammation and metabolic disorders. Nature 444, 860–867.

Ji, H., and Wong, W.H. (2006). Computational biology: toward deciphering gene regulatory information in mammalian genomes. Biometrics 62, 645–663.

Jimenez, M.A., Akerblad, P., Sigvardsson, M., and Rosen, E.D. (2007). Critical role for ebf1 and ebf2 in the adipogenic transcriptional cascade. Mol. Cell. Biol. 27, 743–757.

Krebs, J.E., and Peterson, C.L. (2000). Understanding "active" chromatin: a historical perspective of chromatin remodeling. Crit. Rev. Eukaryot. Gene Expr. 10, 1–12.

Lohoff, M., and Mak, T.W. (2005). Roles of interferon-regulatory factors in T-helper-cell differentiation. Nat. Rev. Immunol. 5, 125–135.

McArthur, M., Gerum, S., and Stamatoyannopoulos, G. (2001). Quantification of DNaseI-sensitivity by real-time PCR: quantitative analysis of DNaseI-hypersensitivity of the mouse beta-globin LCR. J. Mol. Biol. 313, 27–34.

Melillo, R.M., Pierantoni, G.M., Scala, S., Battista, S., Fedele, M., Stella, A., De Biasio, M.C., Chiappetta, G., Fidanza, V., Condorelli, G., et al. (2001). Critical role of the HMGI(Y) proteins in adipocytic cell growth and differentiation. Mol. Cell. Biol. 21, 2485–2495.

Mori, T., Sakaue, H., Iguchi, H., Gomi, H., Okada, Y., Takashima, Y., Nakamura, K., Nakamura, T., Yamauchi, T., Kubota, N., et al. (2005). Role of Kruppel-like factor 15 (KLF15) in transcriptional regulation of adipogenesis. J. Biol. Chem. 280, 12867–12875.

Negre, N., Lavrov, S., Hennetin, J., Bellis, M., and Cavalli, G. (2006). Mapping the distribution of chromatin proteins by ChIP on chip. Methods Enzymol. 410, 316–341.

Oishi, Y., Manabe, I., Tobe, K., Tsushima, K., Shindo, T., Fujiu, K., Nishimura, G., Maemura, K., Yamauchi, T., Kubota, N., et al. (2005). Kruppel-like transcription factor KLF5 is a key regulator of adipocyte differentiation. Cell Metab. 1, 27–39.

Rosen, E.D., and MacDougald, O.A. (2006). Adipocyte differentiation from the inside out. Nat. Rev. Mol. Cell Biol. 7, 885–896.

Ruan, H., Pownall, H.J., and Lodish, H.F. (2003). Troglitazone antagonizes tumor necrosis factor-alpha-induced reprogramming of adipocyte gene expression by inhibiting the transcriptional regulatory functions of NF-kappaB. J. Biol. Chem. 278, 28181–28192.

Sabo, P.J., Humbert, R., Hawrylycz, M., Wallace, J.C., Dorschner, M.O., McArthur, M., and Stamatoyannopoulos, J.A. (2004). Genome-wide identification of DNaseI hypersensitive sites using active chromatin sequence libraries. Proc. Natl. Acad. Sci. USA 101, 4537–4542.

Sabo, P.J., Kuehn, M.S., Thurman, R., Johnson, B.E., Johnson, E.M., Cao, H., Yu, M., Rosenzweig, E., Goldy, J., Haydock, A., et al. (2006). Genome-scale mapping of DNase I sensitivity in vivo using tiling DNA microarrays. Nat. Methods 3, 511–518.

Schones, D.E., Smith, A.D., and Zhang, M.Q. (2007). Statistical significance of cis-regulatory modules. BMC Bioinformatics 8, 19.

Shi, H., Kokoeva, M.V., Inouye, K., Tzameli, I., Yin, H., and Flier, J.S. (2006). TLR4 links innate immunity and fatty acid-induced insulin resistance. J. Clin. Invest. *116*, 3015–3025.

Smith, A.D., Sumazin, P., and Zhang, M.Q. (2005). Identifying tissue-selective transcription factor binding sites in vertebrate promoters. Proc. Natl. Acad. Sci. USA *102*, 1560–1565.

Tanaka, H., Zhao, Y., Wu, D., and Hersh, L.B. (1998). The use of DNase I hypersensitivity site mapping to identify regulatory regions of the human cholinergic gene locus. J. Neurochem. *70*, 1799–1808.

Taniguchi, T., Ogasawara, K., Takaoka, A., and Tanaka, N. (2001). IRF family of transcription factors as regulators of host defense. Annu. Rev. Immunol. *19*, 623–655.

Tong, Q., Dalgin, G., Xu, H., Ting, C.N., Leiden, J.M., and Hotamisligil, G.S. (2000). Function of GATA transcription factors in preadipocyte-adipocyte transition. Science *290*, 134–138.

Tontonoz, P., Hu, E., Graves, R.A., Budavari, A.I., and Spiegelman, B.M. (1994). mPPAR gamma 2: tissue-specific regulator of an adipocyte enhancer. Genes Dev. *8*, 1224–1234.

Villar-Garea, A., and Imhof, A. (2006). The analysis of histone modifications. Biochim. Biophys. Acta *1764*, 1932–1939.

Weinmann, A.S. (2004). Novel ChIP-based strategies to uncover transcription factor target genes in the immune system. Nat. Rev. Immunol. *4*, 381–386.

Wu, J., Srinivasan, S.V., Neumann, J.C., and Lingrel, J.B. (2005). The KLF2 transcription factor does not affect the formation of preadipocytes but inhibits their differentiation into adipocytes. Biochemistry *44*, 11098–11105.